DFT-SQM Force Field for Nickel Porphine: Intrinsic Ruffling

Pawel M. Kozlowski,[†] Thomas S. Rush III,[†] Andrzej A. Jarzecki,[‡] Marek Z. Zgierski,[§] Bruce Chase,[∥] Christine Piffat,[†] Bao-Hui Ye,[⊥] Xiao-Yuan Li,[⊥] Peter Pulay,[⊗] and Thomas G. Spiro*,[†]

Department of Chemistry, Princeton University, Princeton, New Jersey 08540, Department of Chemistry, Indiana University, Bloomington, Indiana 47405, Steacie Institute for Molecular Sciences, National Research Council of Canada, Ottawa, Ontario, Canada K1A OR6, DuPont Experimental Station, Wilmington, Delaware 19880, Department of Chemistry, The Hong Kong University of Science and Technology, Clear Water Bay, Kowloon, Hong Kong S.A.R., China, and Department of Chemistry, University of Arkansas, Fayetteville, Arkansas 72701

Received: April 23, 1998; In Final Form: December 15, 1998

Nonlocal density functional theory [DFT] has been used to compute vibrational frequencies and intensities of nickel porphine and of several isotopomers via a scaled quantum mechanical [SQM] force field [FF]. The results support and extend those obtained from a revised empirical FF. The force constants are similar for the two FF's, although the SQM FF has a complete set of off-diagonal elements. The SQM FF produces somewhat more accurate frequencies and isotope shifts than the empirical FF for the in-plane NiP modes. In addition, the SQM FF calculates out-of-plane modes that are in good agreement with available infrared [IR] data. Also, the SQM FF satisfactorily reproduces the relative intensities of both IR and [off-resonance] Raman bands. A striking result is the calculation of large Raman intensities for nontotally symmetric B_{1g} modes, in conformity with experimental FT-Raman spectra. This effect is attributed to the phasing of local polarizability components of the pyrrole rings and methine bonds. The DFT-computed bond distances and angles are in good agreement with crystallographically determined values. The lowest energy structure is a true minimum with D_{2d} symmetry. It is slightly distorted from the planar geometry along the ruffling coordinate. Constraining it to be planar [D_{4h}] raises the energy slightly [$\sim$0.1 kcal/mol] and leads to an imaginary frequency for the ruffling mode. This finding provides theoretical confirmation of Hoard's empirical observation that metal ions with M−N[pyrrole] bonds significantly shorter than 2.00 Å produce an out-of-plane distortion of the macrocycle. The computed degree of ruffling is small, as are the calculated shifts in vibrational frequencies [<6 cm^{-1}]. Although the symmetry lowering relaxes selection rules, the induced intensity in IR- or Raman-forbidden modes is calculated to be negligible, except for a single IR band associated with an out-of-plane mode [E_g, 420 cm^{-1}], which is indeed observed experimentally. The agreement of both frequencies and intensities with experiment provides further validation of the accuracy of the DFT, even for molecules as complex as metalloporphyrins.

Introduction

The vibrational spectra of metalloporphyrins are of continuing interest because of their utility in probing the structure and dynamics in heme proteins[1] and also because of novel spectroscopic phenomena that are manifested. The high molecular symmetry constrains selection rules and exposes complex and interesting vibronic phenomena in the electronic and resonance Raman [RR] spectra.[2] To extract the information contained in these spectra, one needs a reliable force field [FF], and this has been the target of numerous studies.[3−14] FF construction has been aided by the unusually detailed vibrational mode assignments that are available through variable-wavelength RR spectra, together with isotope labeling.[3,4,9−13] In addition, the analysis of spectra from porphyrins with different peripheral substituents has facilitated the construction of a consistent force field for the porphyrin ring, which accounts for a wide range of data.[13]

Despite these advances, the empirical approach to FF construction is plagued with the well-known difficulty that the numerous possible force field elements of large molecules are underdetermined. In addition, the complex interdependence of these elements makes accurate data fitting tedious and uncertain. For metalloporphyrins, there is the additional problem that most of the out-of-plane vibrations are weak or inactive in either IR or Raman spectra;[2] yet the out-of-plane FF is an important determinant of porphyrin structure and dynamics. In the present work, we make an effort to improve the empirical FF for nickel porphine, the simplest representative of the class [Figure 1], and then turn to ab initio methods.

The remarkable recent advances in ab initio computation have put the potential surfaces and force field [FF] of molecules as large as metalloporphyrins within reach.[15−23] However, the level of theory must be appropriate to the task. For example, the Hartree−Fock (HF) method is inadequate for quantitative porphyrin calculations because it produces a broken symmetry resonance structure.[15,19−21] Inclusion of correlation energy leads

[†] Princeton University.
[‡] Indiana University.
[§] Steacie Institute for Molecular Sciences.
[∥] DuPont Experimental Station.
[⊥] The Hong Kong University of Science and Technology.
[⊗] University of Arkansas.

10.1021/jp9819700 CCC: $18.00
Published on Web 02/20/1999

TABLE 1: Empirical NiP Force Field

stretching terms		bending terms	
K(C_m−H)	5.020	H(C_α−C_m−H)	0.475
K(C_α−C_β)	5.432	H(C_α−C_β−C_β)	1.245
K(C_α−C_m)	6.934	H(H−C_β−C_α)	0.456
K(C_α−N)	5.888	H(C_α−C_m−C_α)	1.253
K(C_β−C_β)	7.353	H(C_α−N−C_α)	1.487
K(C_β−H)	5.200	H(C_α−N−Ni)	0.242
K(N−Ni)	1.880	H(C_β−C_α−C_m)	0.724
		H(C_β−C_α−N)	1.677
		H(H−C_β−C_β)	0.456
		H(C_m−C_α−N)	0.724
		H(N−Ni−N)	0.364

Interaction Terms

1,2 Stretch−Stretch

(C_α−C_m)(C_α−C_β) = 0.600; (C_α−C_m)(C_α−C_m) = 0.700; (C_α−N)(C_α−C_m) = 0.490; (C_α−N)(C_α−C_β) = (C_α−N)(C_α−N) = 0.550; (C_β−C_β)(C_α−C_β) = 0.480; (N−Ni)(C_α−N) = (N−Ni)(N−Ni) = 0.100

1,3 Stretch−Stretch

(C_α−C_β)(C_α−C_β) = (C_β−C_β)(C_α−N) = 0.260; (C_α−C_β)(C_α−N) = 0.050; (N−Ni)(C_α−C_β) = 0.120; (N−Ni)(C_α−C_m) = (N−Ni)(C_α−N) = 0.120; (C_α−C_β)(C_α−C_m) = −0.260; (C_α−C_m)(C_β−C_β) = −0.230; (C_α−C_m)(C_α−N) = −0.090

Bend−Bend Sharing Two Atoms

(C_m−C_α−N)(C_β−C_α−N) = (C_α−C_m−H)(C_α−C_m−C_α) = 0.060; (C_α−N−Ni)(C_α−N−Ni) = (C_α−N−Ni)(C_α−N−C_α) = 0.060; (C_α−C_β−C_β)(H−C_β−C_α) = (C_α−C_β−C_β)(H−C_β−C_β) = 0.030; (H−C_β−C_β)(H−C_β−C_α) = 0.030; (C_m−C_α−N)(C_β−C_α−C_m) = −0.050; (C_β−C_α−N)(C_β−C_α−C_m) = −0.030; (C_α−C_m−H)(C_α−C_m−H) = −0.030; (C_m−C_α−N)(C_α−C_m−C_α) = −0.100; (C_β−C_α−N)(C_α−C_β−C_β) = −0.100; (C_m−C_α−N)(C_α−C_m−H) = −0.100; (C_m−C_α−N)(C_α−N−C_α) = −0.080; (C_β−C_α−N)(C_α−N−C_α) = −0.080; (C_β−C_α−C_m)(C_α−C_m−C_α) = −0.080; (C_α−C_β−C_β)(C_α−C_β−C_β) = −0.070; (C_α−N−Ni)(C_β−C_α−N) = −0.070; (C_α−N−Ni)(C_m−C_α−N) = −0.060; (H−C_β−C_β)(H−C_β−C_β) = −0.050; (C_β−C_α−C_m)(C_α−C_β−C_β) = −0.030; (C_β−C_α−N)(H−C_β−C_α) = 0.040; (C_α−C_m−H)(C_β−C_α−C_m) = 0.100

Bend−Bend Sharing 1 Atom

(C_α−C_β−C_β)(C_α−C_m−C_α) = 0.100; (N−C_α−C_m)(N−C_α−C_m) = 0.100; (C_β−C_α−C_m)(C_β−C_α−C_m) = 0.100

Stretch−Bend with 2 Common Atoms

(C_α−C_β)(C_β−C_α−N) = 0.290; (C_β−C_β)(C_α−C_β−C_β) = 0.270; (C_α−N)(C_m−C_α−N) = (C_α−C_β)(H−C_β−C_α) = 0.250; (C_β−C_β)(H−C_β−C_β) = 0.250; (C_α−C_m)(C_α−C_m−C_α) = 0.240; (C_α−C_β)(C_α−C_β−C_β) = (C_α−N)(C_α−N−C_α) = 0.220; (C_α−C_β)(C_β−C_α−C_m) = (C_α−C_m)(C_m−C_α−N) = 0.200; (C_α−N)(C_β−C_α−N) = (C_α−C_m)(C_α−C_m−H) = 0.200; (N−Ni)(C_a−N−Ni) = (N−Ni)(N−Ni−N) = 0.150

Stretch−Bend with Central Atom Common

(C_α−C_m)(C_β−C_α−N) = (N−Ni)(C_α−N−C_α) = −0.280; (C_α−C_β)(C_m−C_α−N) = −0.250; (C_α−N)(C_β−C_α−C_m) = −0.190; (C_α−N)(C_α−N−Ni) = −0.120; (C_α−C_m)(C_α−C_m−H) = 0.180;(C_α−C_β)(H−C_β−C_β) = (C_β−C_β)(H−C_β−C_α) = 0.050

Stretch−Bend with End Atom Common

(C_α−C_β)(C_α−C_β−C_β) = −0.150; (C_α−C_m)(C_β−C_α−C_m) = (C_α−C_m)(C_m−C_α−N) = −0.120; (C_α−N)(C_α−C_m−C_α) = (C_α−N)(C_m−C_α−N) =−0.120; (C_α−C_β)(C_α−N−C_α) = −0.100; (C_α−N)(C_β−C_α−N) = (C_β−C_β)(C_β−C_α−C_m) = −0.110; (C_β−C_β)(C_β−C_α−N) = −0.110; (C_α−C_m)(C_α−N−Ni) = −0.090; (C_α−C_m)(C_α−C_β−C_β) = (C_α−C_m)(C_α−N−C_α) = −0.080; (C_α−N)(H−C_β−C_α) = −0.060; (C_α−C_β)(C_α−C_m−C_α) = (C_α−N)(C_α−C_β−C_β) = −0.050; (C_α−C_m)(H−C_β−C_α) = −0.020; (C_α−C_β)(H−C_β−C_β) = 0.020; (C_α−N)(C_α−C_m−H) = 0.120; (C_α−C_β)(C_α−C_m−H) = 0.100; (N−Ni)(C_α−N−Ni) = −0.070; (N−Ni)(C_β−C_α−N) = −0.030;

Long−Range

1,8 (C_α−C_m)(C_α−C_m) = −0.170; 1,9 (C_α−C_m)(C_α−C_m) = 0.170

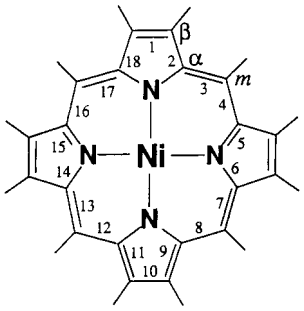

Figure 1. Reference geometry of nickel(II) porphine showing the bond numbering system for one of the 18-membered π delocalization pathways.

to proper bond-equalized structures, as has been demonstrated for free base porphine[15,16] and its magnesium and zinc complexes.[19,20]

Although ab initio potentials systematically overestimate the frequencies of molecular vibrations, the discrepancies can be corrected with a small number of systematically chosen scaling factors.[24] The scaled quantum mechanical [SQM] force field has been successfully applied to numerous small molecules[25,26] and is now applicable to quite large and complex molecules, as the present work and other recent examples[16−19] illustrate. We find that the DFT method reproduces the NiP geometry and vibrational frequencies accurately, and also gives a good qualitative fit to the observed IR and Raman intensities, making assignments unambiguous. The results can be used to evaluate the issue of porphyrin distortion and the activation of out-of-plane modes.

Experimental and Computational Methods

Spectroscopy. Infrared spectra were collected on solid samples of NiP [Midcentry Chemicals (Posen, IL)] in CsI and KBr pellets using Nicolet FTIR spectrometers [models 730 and 800]. Off-resonance Raman spectra were obtained on polycrystalline samples with a Nicolet 950 FT-Raman spectrometer, using laser excitation at 1064 nm [Quantronix 416 Nd:YAG] and 1339 nm [Quantronix 100 Nd:YAG]. Power levels were kept below 200 mW and the samples were examined for photochemical or thermal degradation after each sample run. At 4 cm^{-1} resolution, 500 scans were co-added to improve *S*/*N*. All spectra were corrected for the instrument response function using an NBS traceable incandescent source.

Computational Methods. Calculations were performed using density functional theory [DFT] with the Becke−Lee−Young−Parr composite of exchange-correlation functional (B3-LYP) as implemented in the Gaussian 94 suite of programs.[27] Most calculations (including the final vibrational analysis) were carried out with the 6-31G(d) basis set for H, C, and N atoms and Ahlrich's VTZ basis set for Ni.[28] Dipole moment derivatives for infrared intensities were evaluated with Gaussian 94. Off-resonance Raman intensities were calculated by finite perturba-

TABLE 2: Observed and Calculated Frequencies (cm^{-1}) for NiP and Its Isotopomers [a,b]

local coordinate	A_{1g}	B_{1g}	A_{2g}	B_{2g}	E_u
$\nu(C_mH)$	ν_1 *3041(0,769,0,778)* 3073(0,801,0,801)			ν_{27} *3041(0,771,0,788)* 3073(0,802,0,802)	ν_{36} *3041(0,770,0,772)* 3073(0,801,0,802)
$\nu(C_\alpha H_m)_{asym}$		ν_{10} **1650(−,8,4,14)** *1659(0,24,1,11)* 1659(0,11,3,13)	ν_{19} **1611(−,13,6,19)** *1616(2,30,2,10)* 1615(0,16,2,18)		ν_{37} **1592(−,−,−,−)** *1580(1,31,2,10)* 1595(0,15,5,22)
$\nu(C_\beta C_\beta)$	ν_2 **1574(−,8,22,28)** *1578(0,11,14,31)* 1585(0,7,22,31)	ν_{11} **1505(−,1,51,51)** *1510(0,2,36,42)* 1521(0,2,51,53)			ν_{38} **1547(−,4,20,27)** *1551(1,9,19,35)* 1558(1,6,23,31)
$\nu(C_\alpha C_m)_{sym}$	ν_3 **1459(−,3,28,32)** *1456(0,9,20,30)* 1469(0,6,28,32)			ν_{28} **1505(−,28,18,24)** *1503(6,11,13,22)* 1504(3,7,15,23)	ν_{39} **1462(−,4,42,42)** *1470(5,10,23,30)* 1467(0,2,41,44)
ν(Pyr quarter-ring)			ν_{20} **1354(−,7,41,76)** *1345(−,0,1,489)* 1356(0,5,30,72)	ν_{29} **1368(−,0,44,53)** *1363(0,0,55,55)* 1365(3,3,36,38)	ν_{40} **1385(−,12,−,−)** *1377(10,2,30,39)* 1397(7,44,4,45)
ν(Pyr half-ring)$_{sym}$	ν_4 **1376(−,2,9,9,)** *1374(2,2,22,23)* 1384(8,1,9,9)	ν_{12} **1383(−,62,59,68)** *1324(11,4,13,26)* 1394(6,63,66,65)			ν_{41} **1319(−,4,54,54)** *1331(12,4,36,39)* 1322(2,1,45,52)
$\delta(C_mH)$		ν_{13} **1185(−,247,6,237)** *1200(1,252,1,267)* 1193(2,247,5,241)	ν_{21} **1139(−,229,117,291)** *1119(1,257,17,272)* 1142(7,227,−116,296)		ν_{42} **1150(−,−,54,204)** *1132(2,236,−62,247)* 1151(7,182,57,203)
$\nu(C_\beta H)_{sym}$	ν_5 *3097(0,0,778,778)* 3100(0,0,772,791)	ν_{14} *3097(0,0,779,779)* 3100(0,0,773,791)			ν_{43} *3100(0,0,773,778)* 3120(0,0,791,791)
ν(Pyr half-ring)$_{asym}$			ν_{22} **1005(−,−7,−90,−184)** *1002(4,−11,−206,−195)* 1006(13,−7,−93,−186)	ν_{30} **1062(−,−,−,−)** *1062(19,21,−22,2)* 1062(20,14,96,−10)	ν_{44} **1037(−,10,126,−)** *1031(13,−5,−60,−122)* 1037(16,11,126,142)
$\nu(C_\beta H)_{asym}$			ν_{23} *3095(0,0,785,789)* 3101(0,0,811,811)	ν_{31} *3095(0,0,748,789)* 3101(0,0,812,812)	ν_{45} *3095(0,0,785,790)* 3101(0,0,812,812)
δ(Pyr def)$_{asym}$			ν_{24} **806(−,23,18,39)** *794(0,27,19,46)* 808(0,23,19,36)	ν_{32} **819(−,4,20,39)** *826(0,6,48,54)* 825(0,8,25,60)	ν_{46} **806(−,−,−,−)** *813(1,13,28,37)* 806(1,11,37,42)
ν(Pyr breathing)	ν_6 **995(−,3,8,10)** *1003(20,1,−4,9)* 998(19,2,8,10)	ν_{15} **1003(−,−17,−,−)** *1022(14,0,−2,−6)* 999(15,−21,15,−24)			ν_{47} **995(−,−4,12,−3)** *1010(20,−3,−8,12)* 993(15,−5,9,3)
δ(Pyr def)$_{sym}$	ν_7 **732(−,21,12,23)** *737(0,22,11,24)* 732(0,22,6,25)	ν_{16} **732(−,67,27,77)** *728(3,67,12,76)* 740(3,69,32,78)			ν_{48} **745(−,46,45,67)** *740(1,50,27,68)* 746(1,52,35,68)
δ(Pyr rot.)			ν_{25} **429(−,10,25,32)** *440(1,1,22,24)* 437(4,10,23,32)	ν_{33} **435(−,3,36,36)** *420(0,0,35,35)* 427(0,0,35,35)	ν_{49} **366(−,−,−,−)** *363(3,2,17,19)* 371(3,6,5,11)
ν(NiN)	ν_8 **369(−,2,9,10)** *384(2,1,8,8)* 362(3,1,10,9)	ν_{18} **237(−,0,5,5)** *254(1,0,4,4)* 233(2,0,4,4)			ν_{50} **420(−,−,−,−)** *429(2,1,9,12)* 411(1,1,19,20)
$\delta(C_\beta H)_{asym}$			ν_{26} **1317(−,68,466,405)** *1303(8,32,8,467)* 1329(5,72,476,415)	ν_{34} **1195(−,0,−,245)** *1195(0,1,226,224)* 1193(7,1,109,233)	ν_{51} **1250(−,−,−,−)** *1271(2,34,356,369)* 1263(6,40,38,121)
$\delta(C_\beta H)_{sym}$	ν_9 **1066(−,1,291,293)** *1059(1,3,296,298)* 1067(2,0,294,297)	ν_{17} **1058(−,−22,292,292)** *1060(0,−9,299,287)* 1062(0,−18,292,294)			ν_{52} **1064(−,−4,270,300)** *1058(1,2,299,299)* 1061(1,−4,267,292)
δ(Pyr trans)				ν_{35} **− (−,−,−,−)** *198(2,3,1,3)* 232(2,3,2,5)	ν_{53} **289(−,−,−,−)** *283(0,2,5,5)* 293(0,0,9,9)

[a] ν_x **Freq(**ΔN,[15] $\Delta d4$, $\Delta d8$, $\Delta d12$) ← experiment. *Freq(*ΔN,[15] $\Delta d4$, $\Delta d8$, $\Delta d12$) ← empirical FF. Freq(ΔN,[15] $\Delta d4$, $\Delta d8$, $\Delta d12$) ← SQM FF. [b] Reassigned experimental frequencies are underlined.

TABLE 3: Scaling Factors Used in Scaled Quantum Mechanical Force Field[a]

coordinate type	scale factor
C−N, C−C or Ni−N stretches	0.9337
C−H stretches	0.9122
ring symmetrized deformations	0.9880
CH in plane rockings	0.9340
ring symmetrized torsions	0.9619
out-of-plane modes	0.9486

[a] Scaling factors optimized on free base porphine and its isotopomers ref 17.

tion theory as the numerical second derivative of the nuclear forces with respect to a finite electric field.[18,29,30] Vibrational analysis, including generation of internal coordinates, transformation of Cartesian force constants, and scaling, was performed with the TEXAS suite of programs for electronic structure calculations.

Results and Discussion

Empirical FF. By correlating the RR and IR spectra of nickel complexes of porphine, tetraphenylporphine [TPP], and octaethylporphyrin [OEP], Li et al.[9,10] constructed a valence FF, which was nearly independent of the substituents and accounted satisfactorily for most of the mode frequencies and isotope shifts. Certain discrepancies were ironed out in a subsequent study of nickel etioporphyrin [NiEtio] by Hu et al.[13] We have since been

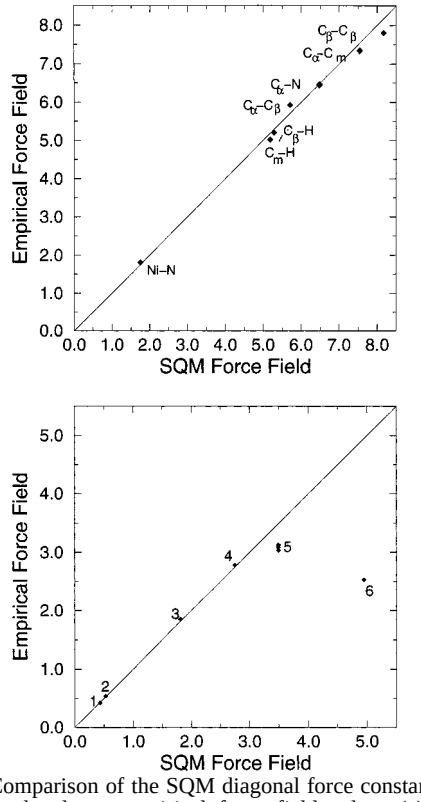

Figure 2. Comparison of the SQM diagonal force constants (x) with the generalized valence empirical force field values (y) using the transformation $\mathbf{F}_{SQM-DFT} = \mathbf{U}^T\mathbf{F}_{EFF}\mathbf{U}$, where the transformation matrix $\mathbf{U}$ is defined in ref 17: (a) stretchings (aJ/Å^2); (b) deformations (aJ/rad^2). Points: (1) $C_\alpha C_\beta H$; (2) $C_\alpha C_m H$; (3) $\sum p_i\{C_\beta C_\alpha N\}_i$, ($p_1 = 1.0$, $p_2 = -p_5 = -0.809017$, $p_3 = -p_4 = 3.09017$); (4) $\sum q_i\{C_\alpha NC_\alpha\}_i$, ($q_1 = -q_4 = 0.587785$, $q_2 = -q_3 = -0.951056$); (5) $NC_\alpha C_m$, (6) $\sum s_i\{C_\alpha C_m C_\alpha\}_i$; ($s_1 = -s_2 = s_3 = -s_4 = 1.0$).

concerned with some remaining discrepancies in the case of NiTPP,[9] and we have readjusted the NiP and NiTPP FF's in a uniform manner using the newer results of Hu et al.[13] The NiTPP reassignments will be presented in a subsequent paper. Table 1 lists the empirical FF elements for NiP, while Table 2 compares observed and calculated frequencies and isotope shifts. The root-mean-square deviation is 3.7% for 143 observed frequencies. Most of the calculated isotope shifts are of the right magnitude, but there remain several significant deviations.

Table 2 is organized according to local coordinate contributions[8,9] and by symmetry [within the D_{4h} point group] to facilitate frequency comparisons. The mode assignments are mostly the same as those in ref 9, but a few experimental bands have been reassigned based on new data and the SQM calculations, as described below.

SQM FF. Table 2 also lists the in-plane frequencies calculated via the SQM-DFT method for a planar NiP molecule at the D_{4h} optimized geometry using four standard SQM scaling constants [Table 3]. The root-mean-square deviation from the observed frequencies is found to decrease to 1.6%, and a number of isotope shift discrepancies are now diminished. For example, the β-d_8 and -d_{12} shifts of the ν_4 mode are now correctly calculated at -9 cm^{-1}, whereas the empirical FF calculation is -23 cm^{-1}.

The empirical and SQM FF's are compared graphically in Figures 2 and 3, after transformation to a common set of nonredundant internal coordinates.[17] The usual redundant coordinates cannot be used for this comparison because they are not defined uniquely by the FF. The stretching coordinates are unaffected, but the force constants for the bending of angles

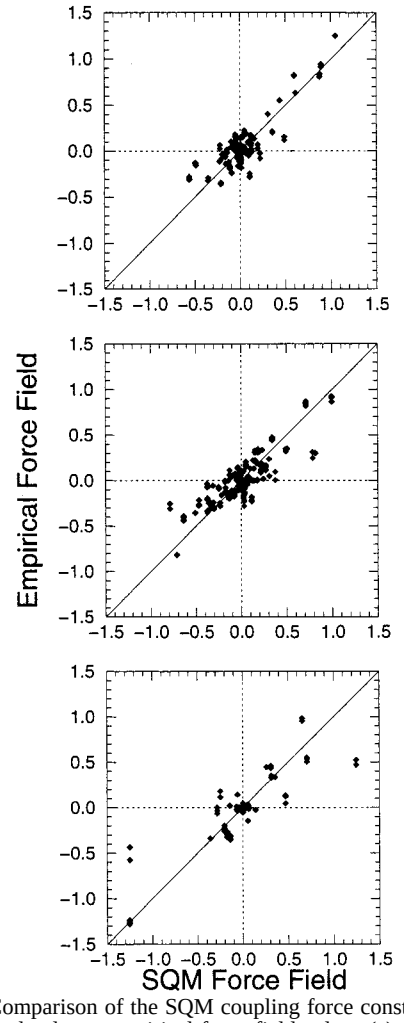

Figure 3. Comparison of the SQM coupling force constants (x) with the generalized valence empirical force field values (y): (a) stretch−stretch couplings (aJ/Å^2); (b) stretch−deformation couplings (aJ/Årad); (c) deformation−deformation couplings (aJ/rad^2).

within the ring structure refer to linear combinations, as given in the Figure 2 caption, and therefore have elevated values.

The principal bond stretching force constants are seen to be in excellent agreement between the empirical and SQM FF's, as are most of the angle bending constants. However, the empirical $C_\alpha C_m C_\alpha$ bending constant is underestimated, probably as a result of compensation by some of the off-diagonal interaction constants.

As might be expected, the off-diagonal force constants are less well correlated [Figure 3] then the diagonal ones. Because these cannot all be constrained by the data, the empirical approach requires setting some remote off-diagonal FF elements to zero and/or constraining chemically similar interactions to be the same. This is a necessarily subjective procedure. The ab initio calculation avoids these approximations and evaluates all the off-diagonal elements. Many of them are in fact very small, but they can have a cumulative impact on the frequencies. It is reassuring to note, however, that no off-diagonal elements were neglected in the empirical FF which have substantial ab initio values. We conclude from the quality of the fit that the empirical FF is a reasonable approximation to the true FF, but the SQM FF is a better approximation.

It is of interest to examine the stretch−stretch interaction constants around the large aromatic ring of porphyrin. Figure 4 gives a plot of these constants in a sequence corresponding to one of the 18-membered conjugation pathways [bond numbering shown in Figure 1]. These results can be compared with the

TABLE 4: Calculated and Observed[a] Out-of-Plane Frequencies (cm^{-1}) for NiP and Its Isotopomers

local coordinate	A_{1u}	A_{2u}	B_{1u}	B_{2u}	E_g
$\gamma(H_mC_\alpha C_mC_\alpha)$[b]		γ_4 855(0,208,8,206)	γ_{10} 891(0,7,43,121)		γ_{19} 842(0,226,−5,194)
		854(−,208,5, −)			**844(−,228,−,−)**
Pyr fold$_{asym}$	γ_1 677(0,0,72,72)		γ_{11} 829(0,95,99,169)		γ_{20} 773(1,−17,42,40)
					776(−,−8, 39,42)
Pyr fold$_{sym}$		γ_5 767(3,−29,22,0)		γ_{15} 652(7,0,106,106)	γ_{21} 888(0,4,151,120)
		768(−,−27,31,4)			896(−,2,152,−)
Pyr swivel			γ_{12} 693(0,97,50,105)		γ_{22} 420(1,19,21,39)
418(−,−,−, −)					
Pyr. tilt				γ_{16} 259(6,0,9,9)	γ_{23} 662(3, −7,111,112)
357(−,−,−,−)	**656(−,−13,104,−)**				
$\gamma(C_mC_\alpha H_mC_\alpha)$[b]		γ_7 705(5,0,141,143)	γ_{13} 460(0,13,32,43)		γ_{24} 700(3,−20,75,96)
698(−,0,131,131)					
$(H_\beta C_\beta - C_\beta H_\beta)_{sym}$		γ_6 282(0,10,6,16)		γ_{17} 780(1,0,66,66)	γ_{25} 229(4,2,8,10)
282(−, −, −, −)					
$(H_\beta C_\beta - C_\beta H_\beta)_{asym}$	γ_2 882(0,0,137,137)				
propeller	γ_3 271(0,0,17,17)				
dome		γ_9 107(0,0,5,5)			
108(−, −, −, −)					
ruffle			γ_{14} 17(i) (0,0,1,1)		
saddle				γ_{18} 43(0,0,2,2)	
wave					γ_{26} 141(0,3,6,9)

[a] Labeling as in Table 2. Experimental frequencies from IR spectra. [b] γ(abcd) = bending of atom a out of the plane of bcd, d being the central atom.

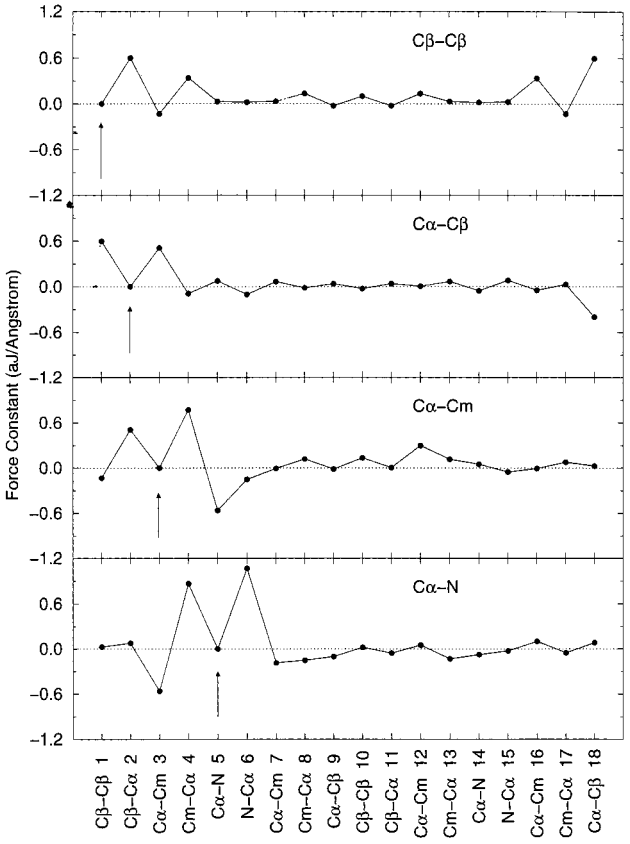

Figure 4. Sretch−stretch coupling constants along the conjugated pathway [see Figure 1 for bond numbering]. The alternating pattern of magnitudes and signs is evident, and interactions across the porphyrin ring are pronounced for the $C_\alpha - C_m$ bonds.

analogous ones obtained for free base porphine.[18] As expected, the interactions connecting successive bonds alternate in sign, with the 1,2 and 1,4 interactions being large and positive and the 1,3 interactions being small and negative. This alternation continues around the conjugation pathway but is greatly attenuated beyond a given pyrrole ring and the adjacent C_m bridges. However, in the case of the $C_\alpha C_m$ bonds, the interactions attain significant values for similar bonds across the porphyrin ring [see values in the third panel for $C_\alpha C_m$ 12 and 13]. This finding lends theoretical support to the inclusion of cross-ring $C_\alpha C_m$ interactions in the empirical FF,[13] which was found to be necessary for proper mode ordering and which was justified by a qualitative argument concerning the resonance structures.

Out-of-Plane Modes. The out-of-plane (oop) porphyrin modes are elusive because D_{4h} selection rules severely restrict their spectroscopic activity. Of the 34 NiP oop modes, only the six A_{2u} modes are IR active. In addition, the eight E_g modes are Raman active, but they are not enhanced in resonance with the dominant $\pi-\pi^*$ transitions [which are polarized in the porphyrin plane], and they have not been reported in off-resonance Raman spectra. The selection rules can, however, be relaxed by symmetry lowering, and the majority of oop modes have been identified in the IR and RR spectra of NiOEP,[11] which can be crystallized in a ruffled conformation. An empirical oop FF was constructed, to support the oop assignments,[11] but its success in reproducing the experimental frequencies was modest. A similar analysis has not been carried out for NiP, for which the data are sparse.

The DFT methodology produces all the normal modes, oop as well as in-plane. The calculated oop frequencies and isotope shifts are listed in Table 4, along with the available data. This table is again organized by symmetry and by local coordinates, except that the five lowest frequency modes are designated by the overall porphyrin distortion to which they lead, following the analysis of Scheidt and co-workers.[31] [The modes are not in frequency order because we wish to maintain correspondence of local coordinates with the mode numbering introduced for NiOEP[11]]. The eigenvectors are illustrated in Figure 5. Two scaling factors, transferred from the free-base porphine calculation,[17] were used for all the oop force constants [Table 3]. The calculated A_{2u} frequencies are all in excellent correspondence with strong IR bands [Figures 6and 7]. In addition, careful inspection of the IR spectra reveal weak bands that are candidates for five of the E_g modes [Table 4], which become IR allowed as a result of NiP ruffling [see below]. However, no oop candidates have been identified in the FT-Raman spectra [Figure 8], and we have been unable to find candidates in either B- or Q-band-excited RR spectra.

Intensities. An important dividend of the ab initio approach is the calculation of relative intensities, for comparison with experiment. The IR intensities are evaluated from the molecular dipole moment derivatives, which are calculated automatically in Gaussian 94.[27] Analytical polarizability derivatives, needed for the Raman intensities, are not yet available in Gaussian 94,

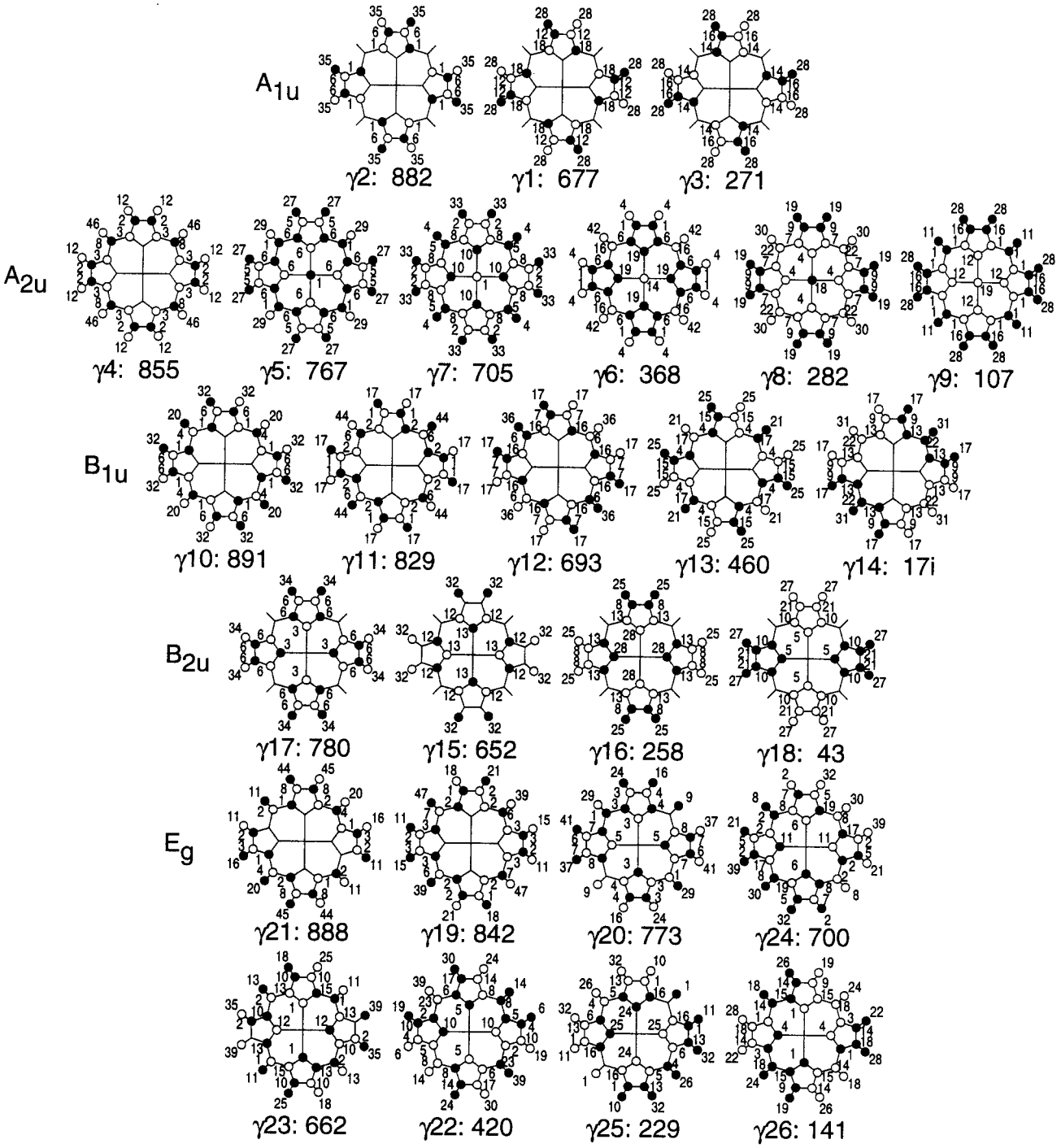

Figure 5. Calculated eigenvectors for the out-of-plane modes of NiP. Open and filled circles indicate displacements above and below the plane of the figure. The numbers indicate the magnitudes of the relative displacements of the atoms.

and thus they were calculated numerically,[29] by applying a small (0.04 au) electric field and calculating the changes in the forces.[18,19,30] The calculated intensities are listed in Tables 5 and 6, and were used to produce the computed spectra in Figures 6−8. The Raman intensities used to simulate the Raman spectrum were corrected for the ω^4 factor. Ab initio calculations, in general, predict high Raman intensities for C−H stretches,[18,30] and the limited experimental data available[32] indicate that such modes are indeed the strongest peaks in the nonresonant Raman spectrum.

For the remaining modes, spectral comparisons [Figures 6−8] show semiquantitative agreement for both FTIR and FT-Raman relative intensities. The overall agreement of the intensity patterns is striking. In no case are weak bands computed to be strong or vice versa. The band assignments are unmistakable. The accuracy of calculated intensities as well as frequencies provides a critical test of the reliability of the SQM FF. However, The DFT calculation underestimates the Raman intensities for ν_8 and ν_{35} [Figure 8], which are by far the strongest bands in the spectrum. These modes have significant contributions from Ni−N(pyrrole) stretching, and it is possible that, because of the complexity of the Ni orbitals, DFT may underestimate the Ni−N bond polarizability. We note that this FF has also produced excellent results in calculating RR intensities of NiP, in conjunction with an INDO-level treatment of the excited states.[33,34]

A point of considerable interest is the calculation of large off-resonant Raman intensities for a series of B_{1g} modes [ν_{10},

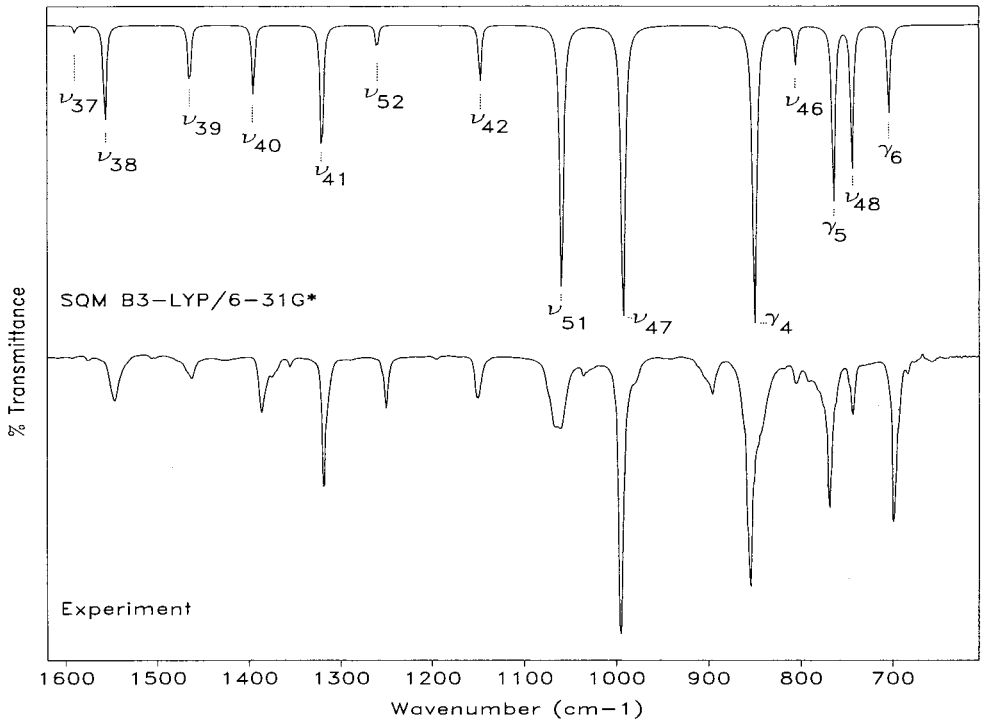

Figure 6. Comparison of experimental IR spectrum of NiP-d_0 with SQM/DFT simulated spectrum with a Lorentzian line profile of 4 cm^{-1} half-width with ω^4 correction in the 500−1800 cm^{-1} frequency range.

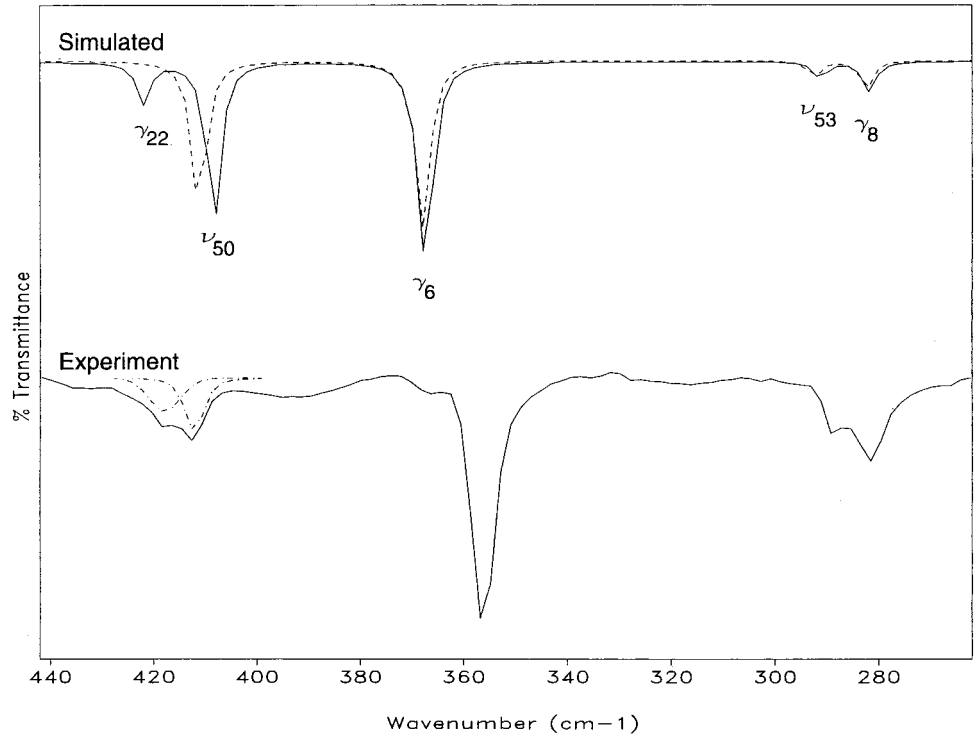

Figure 7. Comparison of experimental IR spectrum of NiP-d_0 with SQM/DFT simulated spectrum with a Lorentzian line profile of 4 cm^{-1} half-width in the 50−550 cm^{-1} frequency range. The solid line is the D_{2d} simulation, while the dashed line is the D_{4h} simulation. A single IR band becomes activated by the ruffling distortion [γ_{22} = 420 cm^{-1}], as is observed experimentally.

ν_{11}, ν_{12}], which are fully supported by the FT-Raman spectrum [Figure 8]. This phenomenon was earlier noted in the FT-Raman spectrum of NiEtio[13] but was unexplained. We considered the possibility of resonance phenomena, but these are unlikely to be significant since the NiEtio absorption spectrum is featureless at the FT-Raman excitation wavelength [1064 nm], and the first allowed electronic transitions are at twice the energy of the excitation. The present calculations establish that the large B_{1g} intensities are intrinsic to the off-resonance polarizability derivatives.

This phenomenon can be understood as a consequence of phasing of the polarizability contributions from the various bonding units in the macrocycle, e.g., the methine bridges or the pyrrole rings. If the polarizability components of individual

TABLE 5: Calculated Raman and IR Band Intensities in D_{2d} Symmetry and the Frequency Downshift (Δ) Upon Ruffling

local coordinate		(I_{Ram})	$\Delta(A_{1g} - A_1)$		(I_{Ram})	$\Delta(B_{1g} - B_1)$		$\Delta(A_{2g} - A_2)$		(I_{Ram}, I_{IR})	$\Delta(B_{2g} - B_2)$		(I_{IR}, I_{ram})	$\Delta(E_u - E)$
$\nu(C_mH)$	ν_1	329.2	4						ν_{27}	199.2, 0.3	4	ν_{36}	12.0, 2.8	4
$\nu(C_\alpha H_m)_{asym}$				ν_{10}	213.9	6	ν_{19}	6				ν_{37}	0.7, 0.2	6
$\nu(C_\beta C_\beta)$	ν_2	282.3	2	ν_{11}	414.0	2						ν_{38}	12.0, 0.1	2
$\nu(C_\alpha C_m)_{sym}$	ν_3	95.0							ν_{28}	6.6, 0.1	2	ν_{39}	7.3, 0.0	2
ν(Pyr quarter-ring)							ν_{20}	2	ν_{29}	87.9, 0.1	0	ν_{40}	7.8, 0.1	1
ν(Pyr half-ring)$_{sym}$	ν_4	8.3	0	ν_{12}	151.3	1						ν_{41}	18.1, 1.0	1
$\delta(C_mH)$				ν_{13}	15.8	3	ν_{21}	2				ν_{42}	6.4, 0.0	3
$\nu(C_\beta H)_{sym}$	ν_5	1111.9	2	ν_{14}	285.2	2						ν_{43}	26.8, 0.7	2
ν(Pyr half-ring)$_{asym}$							ν_{22}	2	ν_{30}	8.1, 0.1	0	ν_{44}	0.0, 0.1	2
$\nu(C_\beta H)_{asym}$							ν_{23}	2	ν_{31}	509.4, 0.3	2	ν_{45}	5.5, 3.6	2
δ(Pyr def)$_{asym}$							ν_{24}	0	ν_{32}	0.2, 0.7	0	ν_{46}	3.8, 0.0	0
ν(Pyr breathing)	ν_6	109.8	0	ν_{15}	1.2	0						ν_{47}	74.2, 0.2	0
δ(Pyr def)$_{sym}$	ν_7	24.3	0	ν_{16}	7.2	0						ν_{48}	17.6, 0.3	2
δ(Pyr rot)							ν_{25}	3	ν_{33}	1.3, 0.1	−1	ν_{49}	0.4, 0.0	1
ν(NiN)	ν_8	125.7	−1	ν_{18}	27.7	2						ν_{50}	6.6, 0.2	3
$\delta(C_\beta H)_{asym}$												ν_{51}	56.5, 0.1	2
$\delta(C_\beta H)_{sym}$	ν_9	104.4	2	ν_{17}	0.7	2	ν_{26}	2	ν_{34}	0.0, 0.2		ν_{52}	2.6, 0.3	2
δ(Pyr trans)									ν_{35}	19.1, 0.1	−1	ν_{53}	0.6, 0.1	1

TABLE 6: Calculated Raman and IR Band Intensities in D_{2d} Symmetry and the Frequency Downshift (Δ) Upon Ruffling

local coordinate		(I_{IRam})	$\Delta(A_{1u} - B_1)$		(I_{Ram}, I_{IR})	$\Delta(A_{2u} - B_2)$		(I_{ram})	$\Delta(B_{1u} - A_1)$	$\Delta(B_{2u} - A_2)$			(I_{IR}, I_{ram})	$\Delta(E_g - E)$
$\gamma(H_mC_\alpha C_mC_\alpha)$				γ_4	0.2, 144.3	5	γ_{10}	1.8	1			γ_{19}	0.0, 1.6	4
Pyr fold$_{asym}$	γ_1	0.1	1				γ_{11}	0.4	4			γ_{20}	0.0, 2.6	1
Pyr fold$_{sym}$				γ_5	0.0, 49.7	3	γ_{15}	1				γ_{21}	0.2, 0.8	1
Pyr. swivel							γ_{12}	0.9	1			γ_{22}	1.9, 0.2	−2
Pyr. tilt				γ_6	0.0, 18.4	1						γ_{23}	0.1, 0.0	1
$\gamma(C_mC_\alpha H_mC_\alpha)$												γ_{24}	0.5, 10.4	2
$(H_\beta C_\beta\text{-}C_\beta H_\beta)_{sym}$										γ_{17}	1	γ_{25}	0.1, 7.3	1
$(H_\beta C_\beta\text{-}C_\beta H_\beta)_{asym}$	γ_2	0.2	1				γ_{13}	0.3	1					
propeller	γ_3	0.2	−1											
dome				γ_9	0.7, 4.6	0								
ruffle							γ_{14}	0.3	*a*					
saddle										γ_{18}	1			
wave												γ_{26}	0.1, 0.1	0

[a] Frequency is 17 cm^{-1} in D_{2d}, 17i cm^{-1} in D_{4h}.

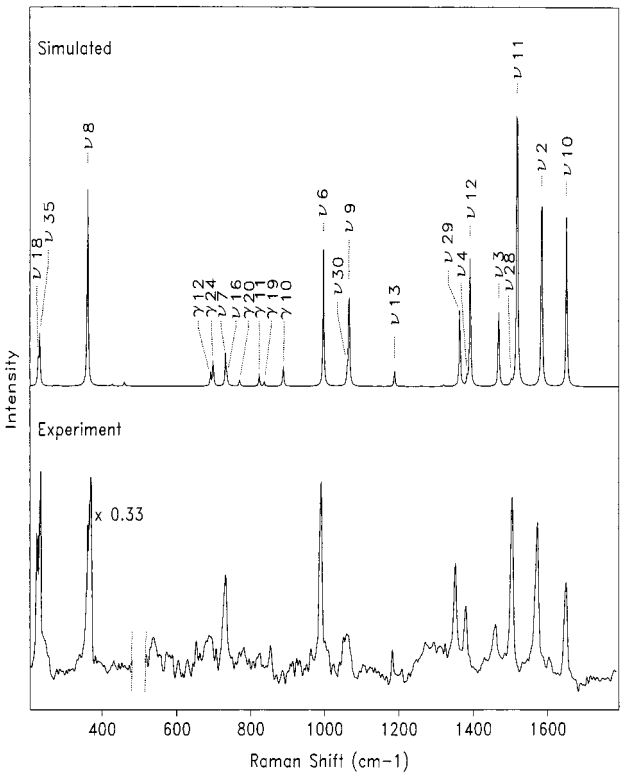

Figure 8. Comparison of experimental off-resonance Raman spectrum of NiP-d_0 with SQM/DFT simulated spectrum with a Lorentzian line profile of 4 cm^{-1} half-width in the 200−1800 cm^{-1} frequency range.

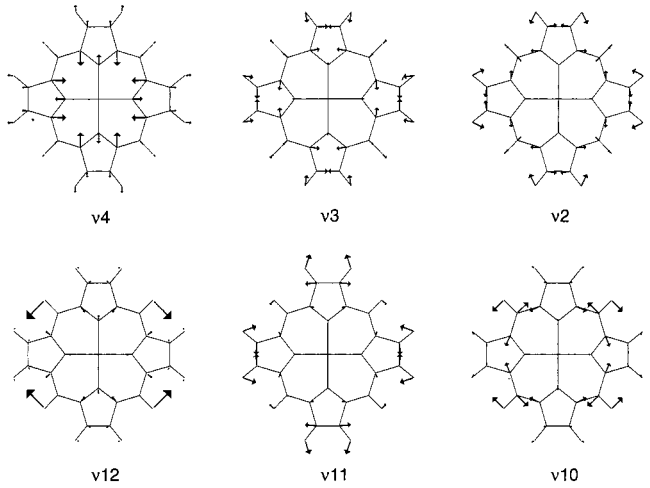

Figure 9. Calculated eigenvectors for selected in-plane modes of NiP.

units are **a** and **b** in directions parallel and perpendicular to the *x* and *y* molecular axis, then the in-plane diagonal polarizability elements are $\alpha_{xx} = \alpha_{yy} = 2(\mathbf{a} + \mathbf{b})$ for A_{1g} modes and $2(\mathbf{a} - \mathbf{b})$ for B_{1g} modes. Large B_{1g} intensities (and small A_{1g} intensities) are therefore expected when **a** and **b** are of opposite signs. This will be the case when the bonding unit distorts in a rectangular fashion so that the local motions are oppositely placed along *x* and *y*. A striking example of this effect is the ν_{12}/ν_4 pair of modes [Figure 9], in which the pyrrole ring is rectangularly distorted; the $C_\alpha N$ bonds expand, while the $C_\alpha C_\beta$ bonds contract. This vibration is one component of an E′ degenerate pair under the approximate D_{5h} symmetry of the pyrrole ring. Consequently, $\mathbf{a} \approx -\mathbf{b}$ and ν_{12} (B_{1g}) is strong, while ν_4 (A_{1g}) is vanishingly weak. In marked contrast, ν_4 is one of the strongest bands in the Soret-excited RR spectrum, because the excited state is displaced along the rectangular pyrrole coordinate.[34] The total polarizability derivative is not relevant for RR scattering, but only the matrix element switch are tied to the resonant excited state. ν_{11} and ν_2/ν_3 are also B_{1g} and A_{1g} modes with rectangular pyrrole distortions (C_α atoms move in while C_β atoms move out Figure 9), and indeed the off-resonant intensity is higher for ν_{11} then ν_2 or ν_3. However, ν_2 and ν_3 do not vanish because they have large contributions (especially ν_2) of in-phase $C_\alpha C_m$ stretching, for which $\mathbf{a} = \mathbf{b}$. The out-of-phase $C_\alpha C_m$

stretching coordinate should produce $\mathbf{a} = -\mathbf{b}$, and the B_{1g} mode made up of coordinate ν_{10} (Figure 9) is also strong. There is no A_{1g} counterpart of ν_{10} since out-of-phase $C_\alpha C_m$ stretching cannot satisfy A_{1g} symmetry.

Reassignments. The assignments of Li et al.[9] are in agreement with the present calculation, except for the few modes listed below.

ν_{12}. As was discovered for NiEtio,[13] this mode is readily detected in the FT-Raman spectrum [Figure 8] but not in RR spectra, because of its overlap with ν_4. Deuteration shifts this mode to a much greater extent than ν_4, and it had earlier been identified in deuterated isotopomers. However, the empirical FF seriously underestimates the deuteration shifts [Table 2] and had predicted too low a natural abundance frequency. This error is corrected by the SQM FF.

ν_{26}. The previous assignment of 848 cm^{-1} for the -d_{12} isotopomer is in error, as noted by Piqueras and Rohlfing.[21] It is reassigned to a band observed experimentally at 912 cm^{-1}.

ν_{34}. This band was not assigned previously, but its predicted frequency, 1195 cm^{-1}, coincides with a band observed by Li et al.[9] in the Q-resonant RR spectra.

ν_{30}. This previously unassigned band is now predicted [1062 cm^{-1}] to overlap with the ν_{17} band. Weak bands at the calculated SQM-FF isotopomer frequencies [Table 2] can be seen in the published Q-resonant RR spectra.

ν_{35}. This mode was listed by Li et al. [9] as being observed at 197 cm^{-1} but is not evident in any of the published spectra. The SQM-FF predicts 232 cm^{-1} for ν_{35}.

ν_{37}. Li et al.[9] assigned this mode to a weak IR band at 1624 cm^{-1}, but there is another weak band at 1592 cm^{-1} [Figure 5] whose position and intensity is in agreement with the present calculation.

Ruffling. Metalloporphyrins are subject to a variety of out-of-plane distortions.[29] These may be due to intermolecular forces [crystal contacts or protein−heme contacts] or to steric clashes of peripheral substituents. In addition, Hoard noted long ago that metalloporphyrins that have the smallest metal ions generally experience a ruffling distortion of porphyrin.[35] He argued that a planar porphyrin has a natural cavity size of 2.00 Å and that metal−N[pyrrole] bonds significantly shorter than this distance would draw the pyrrole rings toward the center through a ruffling distortion of the macrocycle. Since the planar geometry maximizes the π overlap, the equilibrium structure would find a balance between the energy gain from short bonds and the energy penalty to the π system from ruffling. A striking instance of this balance was found for NiOEP, which crystallizes in alternative polymorphs, having either planar or ruffled structures; the Ni−N[pyrrole] distance is 1.958(2) Å (triclinic A) or 1.952 Å (triclinic B) in the planar conformation[36] but 1.929(3) Å in the ruffled conformation.[37] NiOEP ruffling has also been established in solution, via RR spectroscopy, and its extent is temperature-dependent.[11,38]

It is therefore of considerable interest that the DFT calculation for planar NiP yielded an imaginary frequency [Table 4] for γ_{14}, which is in fact the ruffling mode [Figure 7]. When the planar constraint was relaxed along the ruffling coordinate [D_{2d}], the energy was lowered and all vibrational frequencies were positive. Thus, the DFT method lends support to Hoard's explanation of the interplay between metal−N[pyrrole] bond length and the porphyrin planarity. For metals larger than low-spin Ni(II), the DFT method does not show an out-of-plane instability.[19,40] We note that earlier DFT studies on NiP[22,23] did not report nonplanarity effects, emphasizing the importance of adequate functionals.

TABLE 7: Selected DFT Optimized Energies, Bond Lengths (Å) and Bond Angles (deg) of Nickel Porphine Compared with the X-ray Structure

parameter	DFT/6-31G(d),VTZ[a]	DFT/6-311G(d)	X-ray[b]
ΔE (kcal/mol)[c]	0.002	0.105	
Ni−N	1.9659	1.9577	1.951(2)
N−C_α	1.3778	1.3758	1.379(2)
C_α−C_m	1.3823	1.3809	1.371(3)
C_α−C_β	1.4400	1.4386	1.435(4)
C_β−C_β	1.3587	1.3563	1.347(3)
N−Ni−N	90.0	90.00	90.0(1)
Ni−N−C_α	127.66	127.51	127.8(2)
C_α−N−C_α	104.68	104.98	104.3(2)
N−C_α−C_m	125.35	125.22	125.4(3)
N−C_α−C_β	111.06	110.81	111.0(3)
C_β−C_α−C_m	123.55	123.82	123.6(2)
C_α−C_m−C_α	123.58	123.46	123.5(2)
C_α−C_β−C_β	106.60	106.69	106.8(2)
C_α−N−N−C_αd	11.78	19.62	1.7
rms displ[e]	0.1114	0.1833	0.019

[a] 6-31G(d) for H,C,N and Achrlihs VTZ for Ni. [b] From ref 38. [c] $\Delta E = E(D_{2d}) - E(D_{4h})$. [d] Tortional angle (deg) of the opposite pyrrole ring planes with respect to an axis through the nitrogen atoms. [e] Root-mean-square out-of-plane displacement (Å) from the mean plane; definition is given in ref 38.

TABLE 8: Correlation Table for the Species of D_{4h} Group and Its D_{2d} Subgroup

D_{4h}	type[a]				D_{2d}			
A_{1g}	ip		(R)	(RR)	A_1		(R)	(RR)
B_{1u}	oop							
B_{1g}	ip		(R)	(RR)	B_1		(R)	(RR)
A_{1u}	oop							
A_{2g}	ip			(RR)	A_2			(RR)
B_{2u}	oop							
B_{2g}	ip	(IR)	(R)	(RR)	B_2	(IR)	(R)	(RR)
A_{2u}	oop							
E_u	ip	(IR)	(R)		E	(IR)	(R)	
E_g	oop							

[a] ip = in plane; oop = out-of-plane.

The extent of the distortion in NiP is small, as is the energy gain; their magnitude depends on the level of theory [Table 7]. With the 6-31G(d),VTZ basis set, which was used for the vibrational calculations, the gain in energy upon ruffling is trivial and the predicted mean square displacement of the atoms from the porphyrin plane is only 0.1 Å; a more sensitive measure of ruffling, the dihedral angle between the C_α−N bonds on adjacent pyrrole rings[39] is 12°. The larger 6-311G(d) basis set increases this angle to 20° and predicts a 0.1 kcal/mol energy gain. Clearly, the ruffling potential is very soft; the ruffling mode, γ_{14}, has by far the lowest frequency (17 cm^{-1}) of any of normal modes. The calculated frequency shift between the planar and ruffled structures are all less than 6 cm^{-1}. The softness of the potential is supported by a recent crystal structure of NiP,[39] which is almost planar; the reported ruffling angle is only 2°. There are extensive contacts between pairs of molecules in the crystal, which can easily overcome the small ruffling tendency. The calculated bond distances and angles are in good agreement with the reported values [Table 8]; the bond distances are only slightly overestimated.

The calculated and observed intensities provide another test of the ruffling distortion. The symmetry lowering induces activity for modes that are forbidden in the higher symmetry, as summarized in Table 8. However, the calculated intensities of the newly activated modes are all very small, in both the Raman [B_{1u}, A_{1u}, A_{2u}] and IR [E_g] spectra. They are too small to be detected in the Raman spectra, and only one newly activated IR band has significant intensity, namely γ_{22} [E_g], at 420 cm^{-1}. γ_{22} is a swiveling mode of the pyrrole rings and generates a significant dipole in the ruffled structure. This band is in fact detected in the IR spectrum [Figure 6] at about the right intensity. In addition, four other candidate E_g modes can

be detected at high sensitivity, as discussed above. Thus, the DFT calculation gives out-of-plane effects on the intensities that are in good agreement with experiment.

The ruffling distortion in NiP is much smaller than that in the ruffled polymorph of NiOEP [ruffling angle of 32.8°[37]], presumably because the steric clashes of the OEP substituent groups amplify the ruffling effect of the metal. This phenomenon is even more pronounced in sterically crowded porphyrins such as nickel octaethyltetraphenyloporphine [NiOETPP], which show large out-of-plane distortions, especially for the nickel complex.[41] Further DFT analysis of this phenomenon is in progress.

Conclusions

Our results on NiP indicate that DFT at the level of sophistication now available is capable of providing accurate results on even quite subtle features of metallopophyrin electronic structure. Bond distances and angles, as well as normal-mode frequencies and compositions, are all accurately calculable, and computed IR and Raman intensities are in good agreement with experiment. Even the surprisingly high off-resonant Raman intensities of B_{1g} modes are captured by the calculation.

Moreover, the dividing line between planar and nonplanar porphyrins in response to metal ion size is accurately reproduced. NiP happens to be right at that line. The planar structure is unstable with respect to ruffling, but the potential is soft and easily overcome by intermolecular forces. The consequences of the ruffling for spectroscopic activity are accurately calculated; there is no significant activation of Raman bands, despite the symmetry lowering, and only one IR band, the pyrrole swiveling mode, γ_{22}, gains significant intensity. This band is observed experimentally, with the proper relative intensity, whereas other bands arising from D_{2d} activation are very weak, as predicted. Thus DFT is capable of accounting for all significant features of the NiP IR and Raman spectra. It also gives mode compositions that are reliable enough to compute resonance Raman enhancements, in conjunction with INDO-level evaluation of the resonant excited state.[33,34]

Acknowledgment. This work was supported by NIH Grant GM 33576 from the National Institute of General Medical Sciences to T.G.S. and by NSF Grants CHE-88141443 and CHE-9707202 to P.P. Issued as NRCC No. 40906.

References and Notes

(1) Spiro, T. G. *Adv. Protein Chem.* **1985**, *37*, 111.
(2) Li, X.-Y.; Spiro, T. G. In *Biological Applications of Raman Spectroscopy*; Spiro, T. G., Ed.; Wiley-Intersicience: New York, 1988; Vol III, Chapter 1.
(3) Kitagawa, T.; Abe, M.; Oghoshi, H. *J. Chem. Phys.* **1978**, *69*, 4516.
(4) Abe, M.; Kitagawa, T.; Kyogoku, Y. *J. Chem. Phys.* **1978**, *69*, 4516.
(5) Gladkov, L. L.; Solovyov, K. N. *Spectrochim. Acta* **1985**, *41A*, 1437.
(6) Gladkov, L. L.; Solovyov, K. N. *Spectrochim. Acta* **1985**, *41A*, 1443.
(7) Gladkov, L. L.; Solovyov, K. N. *Spectrochim. Acta* **1986**, *42A*, 1.
(8) Spiro, T. G.; Czernuszewicz, R. S.; Li, X.-Y. *Coord. Chem. Rev.* **1990**, *100*, 541.
(9) Li, X.-Y.; Czernuszewicz, R. S.; Kincaid, J. R.; Su, Y. O.; Spiro, T. G. *J. Phys. Chem.* **1990**, *94*, 31.
(10) Li, X.-Y.; Czernuszewicz, R. S.; Kincaid, J. R.; Su, Y. O.; Spiro, T. G. *J. Phys. Chem.* **1990**, *94*, 47.
(11) Li, X.-Y.; Czernuszewicz, R. S.; Kincaid, J. R.; Spiro, T. G. *J. Am. Chem. Soc.* **1990**, *111*, 7012.
(12) Li, X.-Y.; Zgierski, M. Z. *J. Phys. Chem.* **1991**, *95*, 4268.
(13) Hu, S.; Mukherjee, A.; Piffat, C.; W. Mak, R. S.; Li, X.-Y.; Spiro, T. G. *Biospectrosc.* **1995**, *1*, 395.
(14) Procyk, A. D.; Bocian, D. F. *Annu. Rev. Phys. Chem.* **1992**, *43*, 465.
(15) Almlöf, J.; Fischer, T. H.; Gassman, P. G.; Ghosh, A.; Häser, M. *J. Phys. Chem.* **1993**, *97*, 10964.
(16) Kozlowski, P. M.; Zgierski, M. Z.; Pulay, P. *Chem. Phys. Lett.* **1995**, *247*, 379.
(17) Kozlowski, P. M.; Jarzecki, A. A.; Pulay, P. *J. Phys. Chem.* **1996**, *100*, 7007.
(18) Kozlowski, P. M.; Jarzecki, A. A.; Pulay, P.; Li, X. Y.; Zgierski, M. Z. *J. Phys. Chem.* **1996**, *100*, 13985.
(19) Jarzecki, A. A.; Kozlowski, P. M.; Pulay, P.; Ye, B. H.; Li, X. Y. *Spectrochim. Acta* **1996**, *53A*, 1195.
(20) Piqueras, M. C.; Rohlfing, C. M. *J. Mol. Struct. (THEOCHEM)* **1996**, *388*, 293.
(21) Piqueras, M. C.; Rohlfing, C. M. *Theor. Chem. Acc.* **1997**, *97*, 81.
(22) Matsuzawa, N.; Ata, M.; Dixon, D. A. *J. Phys. Chem.* **1995**, *99*, 7698.
(23) Rosa, A.; Baerends, E. J. *Inorg. Chem.* **1994**, *33*, 584.
(24) Pulay, P.; Fogarasi, G.; Pongor, G.; Boggs, J. E.; Vargha, A. *J. Am. Chem. Soc.* **1983**, *105*, 7037.
(25) Fogarasi, G.; Pulay, P. *Annu. Rev. Phys. Chem.* **1984**, *35*, 191.
(26) Pulay, P.; Fogarasi, G.; Zhou, X.; Taylor, P. W. *Vib. Spectrosc.* **1990**, *1*, 159.
(27) Frisch, M. J.; Trucks, G. W.; Schlegel, H. B.; Gill, P. M. W.; Johnson, B. G.; Robb, M. A.; Chesseman, J. R.; Keith, T. A.; Petersson, G. A.; Montgomery, J. A.; Raghavachari, K.; Al-Laham, M. A.; Zakrzewski, V. G.; Ortiz, J. V.; Foresman, J. B.; Cioslowski, J.; Stefanov, B. B.; Nanayakkara, A.; Challacombe, M.; Peng, C. Y.; Ayala, P. Y.; Chen, W.; Wong, M. W.; Andres, J. L.; Replogle, E. S.; Gomperts, R.; Marin, R. L.; Fox, D. J.; Binkley, J. S.; Defrees, D. J.; Baker, J.; Stewart, J. P.; Head-Gordon, M.; Gonzalez, C.; Pople, J. A. *Gaussian 94*; Gaussian Inc.: Pittsburgh, PA, 1995.
(28) Schäfer, A.; Horn, H.; Ahlrichs, R. *J. Phys. Chem.* **1992**, *97*, 2571.
(29) Komornicki, A.; McIver, J. W., Jr. *J. Phys. Chem.* **1979**, *70*, 2014.
(30) Kozlowski, P. M.; Rauhut, G.; Pulay, P. *J. Chem. Phys.* **1995**, *103*, 5650. Porezag, D.; Pederson, M. R. *Phys. Rev. B* **1996**, *54*, 7830.
(31) Scheidt, W. R.; Lee, Y. J. *Structure and Bonding*; Springer: Berlin, 1987; Vol. 64, p 2.
(32) Martin, J.; Montero, S. *J. Chem. Phys.* **198**, *80*, 4610. Gough, K. M.; Murphy, W. F. *J. Chem. Phys.* **1987**, *87*, 1509. Gough, K. M.; Murphy, W. F.; Stoyer-Hensen, T.; Norby Svendsen, E. *J. Chem. Phys.* **1987**, *87*, 3341. Fernandez-Sanchez, J. M.; Montero, S. *J. Chem. Phys.* **1989**, *90*, 2909. Domingo, C.; Escribano, R.; Murphy, W. F.; Montero, S. *J. Chem. Phys.* **1982**, *77*, 4353.
(33) Rush, T., III; Kumble, R.; Mukherjee, A.; Blackwood, M. E., Jr.; Spiro, T. G. *J. Phys. Chem.* **1996**, *100*, 12076.
(34) Kumble, R.; Rush, T. S., III; Blackwood, M. E., Jr., Kozlowski, P. M.; Spiro, T. G. *J. Phys. Chem. B* **1998**, *102*, 7280.
(35) Hoard, J. L. *Science* **1971**, *174*, 1295.
(36) Cullen, D. L.; Meyer, E. F. *J. Am. Chem. Soc.* **1974**, *96*, 2095. Brennan, T. D.; Scheidt, W. R.; Shelnutt, J. A. *J. Am. Chem. Soc.* **1988**, *110*, 3919.
(37) Meyer, E. F., Jr. *Acta Crystalogr., Sect. B* **1972**, *B28*, 2162.
(38) Alden, R. G.; Crawford, B. A.; Doolen, R.; Ondrias, M. R.; Shelnutt, J. A. *J. Am. Chem. Soc.* **1989**, *111*, 2070.
(39) Jentzen, W.; Turowska-Tyrk, I.; Robert Scheidt, W.; Shelnutt, J. A. *Inorg. Chem.* **1996**, *35*, 3559.
(40) Kozlowski, P. M.; Spiro, T. G.; Berces, A.; Zgierski, M. Z. *J. Phys. Chem.*, in press.
(41) Piffat, C.; Melamed, D.; Spiro, T. G. *J. Phys. Chem.* **1993**, *97*, 7441.